Cancer Letters 467 (2019) 96–106

Contents lists available at ScienceDirect

Cancer Letters

journal homepage: www.elsevier.com/locate/canlet

Original Articles

Multi-dimensional immunoproteomics coupled with *in vitro* recapitulation of oncogenic NRAS^{Q61R} identifies diagnostically relevant autoantibody biomarkers in thyroid neoplasia

Pavel V. Belousov[a,*], Marina A. Afanasyeva[a], Ekaterina O. Gubernatorova[a,b], Apollinariya V. Bogolyubova[a,c], Aksinya N. Uvarova[a], Lidia V. Putlyaeva[a,d], Egle-Marija Ramanauskaite[b], Arthur T. Kopylov[e], Denis E. Demin[a,f], Karina A. Tatosyan[a], Alina S. Ustiugova[a,b], Maria M. Prokofjeva[a], Kirill V. Lanshchakov[g,h], Vladimir E. Vanushko[g], Andrew R. Zaretsky[i,j], Natalya V. Severskaia[k], Nina Y. Dvinskikh[k], Alexander Y. Abrosimov[g,l], Dmitry V. Kuprash[a,b], Anton M. Schwartz[a]

[a] *Engelhardt Institute of Molecular Biology, Russian Academy of Sciences, Moscow, Russia*
[b] *Biological Faculty, Lomonosov Moscow State University, Moscow, Russia*
[c] *Center for Genetics and Life Sciences, Educational Center «Sirius», Sochi, Russia*
[d] *Center of Life Sciences, Skolkovo Institute of Science and Technology, Moscow, Russia*
[e] *Institute of Biomedical Chemistry, Moscow, Russia*
[f] *Moscow Institute of Physics and Technology, Moscow, Russia*
[g] *National Medical Research Center for Endocrinology, Ministry of Health of the Russian Federation, Moscow, Russia*
[h] *Central Clinical Hospital of the Presidential Administration of the Russian Federation, Moscow, Russia*
[i] *Shemyakin-Ovchinnikov Research Institute for Bioorganic Chemistry, Russian Academy of Sciences, Moscow, Russia*
[j] *Evrogen Lab LLC, Moscow, Russia*
[k] *Tsyb Medical Radiological Research Center, Ministry of Health of the Russian Federation, Obninsk, Russia*
[l] *National University of Science & Technology «MISIS», Moscow, Russia*

ARTICLE INFO

Keywords:
2-dimensional difference gel electrophoresis
Autoantibodies
Biomarkers
Serological proteome analysis
Thyroid neoplasms

ABSTRACT

Tumor-associated antigen (TAA)-specific autoantibodies have been widely implicated in cancer diagnosis. However, cancer cell lines that are typically exploited as candidate TAA sources in immunoproteomic studies may fail to accurately represent the autoantigen-ome of lower-grade neoplasms. Here, we established an integrated strategy for the identification of disease-relevant TAAs in thyroid neoplasia, which combined NRAS^{Q61R} oncogene expression in non-tumorous thyroid Nthy-ori 3–1 cells with a multi-dimensional proteomic technique **DISER** that consisted of profiling NRAS^{Q61R}-induced proteins using 2-dimensional difference gel electrophoresis (2D-**DI**GE) coupled with serological proteome analysis (**SER**PA) of the TAA repertoire of patients with thyroid encapsulated follicular-patterned/RAS-like phenotype (EFP/RLP) tumors. We identified several candidate cell-based (nicotinamide phosphoribosyltransferase NAMPT, glutamate dehydrogenase GLUD1, and glutathione S-transferase omega-1 GSTO1) and autoantibody (fumarate hydratase FH, calponin-3 CNN3, and pyruvate kinase PKM autoantibodies) biomarkers, including NRAS^{Q61R}-induced TAA phosphoglycerate kinase 1 PGK1. Meta-profiling of the reactivity of the identified autoantibodies across an independent SERPA series implicated the PKM autoantibody as a histological phenotype-independent biomarker of thyroid malignancy (11/38 (29%) patients with overtly malignant and uncertain malignant potential (UMP) tumors vs 0/22 ($p = 0.0046$) and 0/20 ($p = 0.011$) patients with non-invasive EFP/RLP tumors and healthy controls, respectively). PGK1 and CNN3 autoantibodies were identified as EFP/RLP-specific biomarkers, potentially suitable for further discriminating tumors with different malignant potential (PGK1: 7/22 (32%) patients with non-invasive EFP/RLP tumors vs 0/38 ($p = 0.00044$) and 0/20 ($p = 0.0092$) patients with other tumors and healthy controls, respectively; CNN3: 9/29 (31%) patients with malignant and borderline EFP/RLP tumors vs 0/31 ($p = 0.00068$) and 0/20 ($p = 0.0067$) patients with other tumors and healthy controls, respectively). The combined use of PKM, CNN3, and PGK1 autoantibodies allowed the reclassification of malignant/UMP tumor risk in 19/41 (46%) of EFP/RLP tumor patients. Taken together, we established an experimental pipeline **DISER** for the concurrent identification

* Corresponding author. 32 Vavilova str., 119991, Moscow, Russia.
E-mail address: belousp@gmail.com (P.V. Belousov).

https://doi.org/10.1016/j.canlet.2019.07.013
Received 28 October 2018; Received in revised form 15 July 2019; Accepted 16 July 2019

of cell-based and TAA biomarkers. The combination of **DISER** with *in vitro* oncogene expression allows further targeted identification of oncogene-induced TAAs. Using this integrated approach, we identified candidate autoantibody biomarkers that might be of value for differential diagnostic purposes in thyroid neoplasia.

Abbreviations

2D-DIGE	2-dimensional difference gel electrophoresis
2D-PAGE	2-dimensional polyacrylamide gel electrophoresis
CCBB	colloidal coomassie brilliant blue
CNN3	calponin-3
cPTC	classic/conventional type of PTC
DISER	2D-**DI**GE + **SER**PA
EFP/RLP	encapsulated follicular-patterned/RAS-like phenotype
emPAI	exponentially modified protein abundance index
EnFV-PTC	encapsulated follicular variant of PTC
ERK	extracellular signal–regulated kinase
FH	fumarate hydratase, mitochondrial
FNAB	fine-needle aspiration biopsy
FTA	follicular thyroid adenoma
FTC	follicular thyroid carcinoma
FT-UMP	follicular tumor of UMP
GLUD1	glutamate dehydrogenase, mitochondrial
GSTO1	glutathione S-transferase omega-1
IDH3A	isocitrate dehydrogenase [NAD] subunit alpha, mitochondrial
MS/MS	tandem mass-spectrometry
NAMPT	nicotinamide phosphoribosyltransferase
NIFTP	non-invasive follicular thyroid neoplasm with papillary-like nuclear features
PGK1	phosphoglycerate kinase 1
PKM	pyruvate kinase PKM
PTC	papillary thyroid carcinoma
PTC-NF	nuclear features of PTC
ROI	region of interest
RTCB	tRNA-splicing ligase RtcB homolog
SERPA	serological proteome analysis
TAA	tumor-associated antigen
UMP	uncertain malignant potential
WB	Western blot analysis
WDT-UMP	well-differentiated tumor of UMP

1. Introduction

Autoantibodies against tumor-associated antigens (TAAs) are blood-based cancer biomarkers that can help detect malignancy with high diagnostic specificity (reviewed in Ref. [1]). The notable clinically validated examples are onconeural autoantibodies, which are routinely used to diagnose the underlying neoplasia in possible paraneoplastic syndromes [2] and *Early*CDT-Lung test for pulmonary nodule risk assessment and lung cancer screening (https://oncimmune.com/lung-cancer-blood-test/). However, despite high research effort, the overall success of these cancer biomarkers remains limited.

One specific limitation encountered in immunoproteomic studies attempting to identify novel autoantibody biomarkers is the use of established cancer cell lines as a renewable and consistent source of bait antigens to capture the circulating antibodies. Compared to primary tumors, cancer cell lines frequently demonstrate a profound loss of their original differentiation, exaggerated epigenetic and karyotypic abnormalities, increased mutational load, and altered gene expression profiles, which result in a poorly differentiated state that is shared between cell lines but distinct from the primary tumors of the same tissue origin (reviewed in Ref. [3]). Consequently, the resultant pool of antigens represents proteins that are associated with a highly malignant undifferentiated phenotype rather than the immunogenic proteomic changes occurring in benign, premalignant, well-differentiated, and early-stage lesions.

Human thyroid tumors have been our primary research interest and their well-differentiated nature ensures the relevance of the above-mentioned considerations. We hypothesized that coupling the activation of a single key oncogenic pathway in non-tumorous thyroid lineage cells with differential proteomic/immunomic profiling of resultant cells may partially overcome the limitation described above by focusing the search strategy on the disease-relevant antigens whose expression is induced by a specific oncogenic event.

Hotspot mutations in the genes of the RAS family of proto-oncogenes, including *NRAS* c.*182A* > *G* (p.Q61R), are common in human thyroid neoplasms and are strongly associated with a particular group of histopathological phenotypes hereinafter collectively referred to as encapsulated follicular-patterned/RAS-like phenotype (EFP/RLP), which includes multiple World Health Organization-recognized pathological entities with varying malignant potential as detailed in Supplementary Table 1 [4–12]. Of note, due to predominantly follicular architecture, the absence or incomplete/focal papillary thyroid carcinoma (PTC) nuclear features (PTC-NF), and inability of the fine-needle aspiration biopsy (FNAB) to assess the presence of microscopic invasive growth, EFP/RLP tumors pose significant diagnostic difficulties, particularly regarding preoperative discrimination between benign and malignant lesions [13]. Furthermore, the value of molecular testing of FNAB specimens in this group of neoplasms is limited since RAS mutations are comparably prevalent in benign, malignant and borderline EFP/RLP tumors, whereas highly predictive of malignancy *BRAF* mutations and RET/PTC rearrangements are only occasionally encountered [4–12]. Thus, novel biomarkers that are capable of addressing these diagnostic issues are required to optimize the management of patients and reduce treatment costs via the avoidance of unnecessary surgeries.

Here, we employed a combination of 1) differential proteomic analysis of two derivates of the immortalized normal human thyroid follicular epithelial cell line, Nthy-ori 3–1, genetically engineered to stably express either the prototype EFP/RLP driver $NRAS^{Q61R}$ or the puromycin resistance gene only, and 2) the autoantibody profiling of sera from EFP/RLP tumor patients using proteins isolated from resultant cell lines as the bait antigen pool. We combined two 2-dimensional polyacrylamide gel electrophoresis (2D-PAGE)-based techniques, the 2D-difference gel electrophoresis (2D-DIGE) [14] and serological proteome analysis (SERPA) [15], into an experimental pipeline, which we named **DISER** (2D-**DI**GE + **SER**PA).

Using this multi-dimensional approach and meta-profiling of the reactivity of the identified autoantigens across a total of five independent SERPA experimental series, we were able to unravel a number of candidate cell-based and circulating autoantibody biomarkers, and further implicate the latter as potential biomarkers for identifying thyroid neoplastic disease (fumarate hydratase, mitochondrial FH), malignant/uncertain malignant potential (UMP) tumors (pyruvate kinase PKM), and the discrimination of EFP/RLP tumors with different malignant potential (calponin-3 CNN3 and $NRAS^{Q61R}$-induced TAA phosphoglycerate kinase 1 PGK1). The combination of PKM, CNN3, and PGK1 autoantibodies allowed the reclassification of malignant/UMP tumor risk in nearly half of EFP/RLP tumor patients.

The **DISER** approach coupled with *in vitro* recapitulation of a specific oncogenic stimulus combines and improves the advantages of the

individual 2D-DIGE and SERPA techniques and may be used for concurrent differential proteomic/immunoproteomic profiling and successful identification of oncogene-induced autoantigens and disease-relevant autoantibody signatures in human neoplasia.

2. Materials and methods

2.1. Patients and samples

The sera samples from most of the patients included in the study were a component of a sample set described previously [16], obtained from the Endocrinology Research Center, currently the National Medical Research Center for Endocrinology, Moscow, Russia (ERC samples); the Tsyb Medical Radiological Research Center, Obninsk, Russia (MRRC samples); and from the outpatient clinic of the Lomonosov Moscow State University (healthy female volunteers without palpable thyroid nodules). Additional samples were obtained either from the National Medical Research Center for Endocrinology (additional ERC samples); or from the Russian repository of the Chernobyl Tissue Bank (https://www.chernobyltissuebank.com/) at the Tsyb Medical Radiological Research Center (MRRC/CTB samples, project number 001/2015). Representative archival hematoxylin and eosin-stained slides corresponding to each case were reviewed by a single board-certified surgical pathologist (AYA), and pathological diagnoses were rendered compliant with the current 4th edition of the World Health Organization classification of tumors of endocrine organs [17] (Supplementary Tables 1 and 2). Basic clinico-pathological characteristics of patients together with other relevant information are presented in Supplementary Table 2. At diagnosis, none of the included patients demonstrated clinical or radiological evidence of gross extrathyroidal extension (T3b or T4) or distant metastases (M1), and no widely invasive EFP/RLP tumors were present in the entire cohort. For simplicity of data presentation, a non-generally accepted term, malignancy score (M-score), was used to describe the histological degree of malignancy as defined in Supplementary Table 1. The mutational status of the *NRAS* gene was determined as described in the Supplementary Methods. All patients provided informed consent; the study was approved by the Ethical Review Boards of the participating institutions.

2.2. Cell lines

Nthy-ori 3-1 (ECACC 90011609), FTC-133 (ECACC 94060901), and K1 (92030501) cells were purchased from the European Collection of Authenticated Cell Cultures (ECACC) via Sigma-Aldrich. The culturing media were DMEM:Ham's F12:MCDB 105 2:1:1 for K1 cells, DMEM:Ham's F12 1:1 for FTC-133 cells, and RPMI 1640 for Nthy-ori 3-1 cells and its derivates. All media were supplemented with 2 mM L-glutamine, 10% fetal bovine serum, and 100 Units/mL penicillin/100 µg/mL streptomycin. For 2D-DIGE comparison of K1, FTC-133, and Nthy-ori 3–1 cells, all cells were adapted to DMEM:Ham's F12 1:1 medium supplemented as described previously for four passages.

The Nthy-ori 3-1-NRAS^{Q61R} and Nthy-ori 3-1-Vector derivates have been described elsewhere [18]. Briefly, full-length mutant NRAS^{Q61R} cDNA was cloned into lentiviral plasmid vector LeGO-iPuro2 carrying the puromycin resistance gene (a generous gift from Dr. Kristoffer Riecken, Medical Center Hamburg-Eppendorf) [19], and viral particles LeGO-iPuro2 and LeGO-iPuro2-NRAS^{Q61R} were produced and used for infection of Nthy-ori 3-1 cells, followed by 14 days of selection using 1 µg/mL puromycin (Fig. 1A).

2.3. 2D-PAGE and Western blot analysis (WB)

Total protein lysate or equimolar mixtures of different cyanine dye-labeled proteins prepared as described in the Supplementary Methods were subjected to isoelectric focusing (Protean IEF cell, Bio-Rad) using 7 cm immobilized pH gradient strips (Bio-Rad) with non-linear pH 3–10 gradient for up to 33 kV h. Strips were equilibrated either for 20 min in reductive equilibration buffer containing 6 M urea, 0.375 M Tris-HCl (pH 8.8), 2% (w/v) sodium dodecyl sulfate (SDS), 20% (w/w) glycerol, and 2% (w/v) dithiothreitol (K1 and FTC-133 proteins), or for 10 min in reductive equilibration buffer and further 10 min in alkylating buffer containing 2.5% (w/v) iodoacetamide instead of dithiothreitol (Nthy-ori 3-1-NRAS^{Q61R} and Nthy-ori 3-1-Vector proteins), and subjected to SDS-PAGE in the second dimension using 10% polyacrylamide gels. Following the detection of fluorescence, if applicable, proteins were stained with colloidal Coomassie Brilliant Blue (CCBB) G-250 stain for spot picking, or were electroblotted onto nitrocellulose membranes and

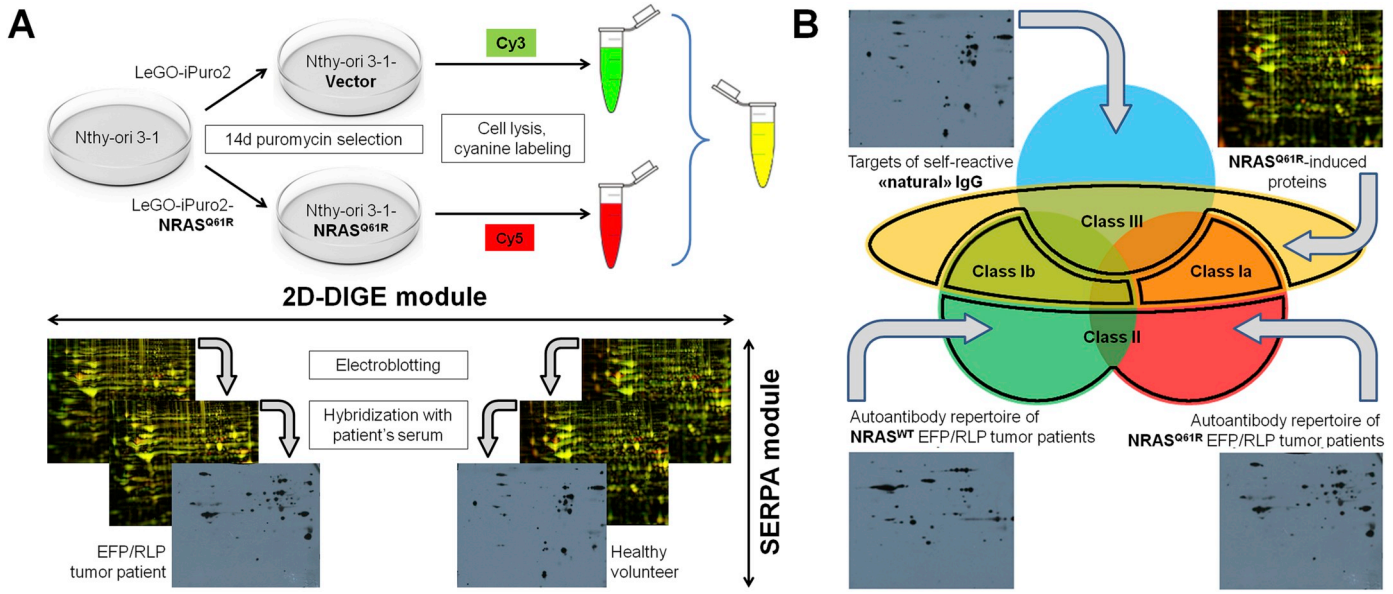

Fig. 1. Schematic representation of the experimental pipeline. A, Establishment of the Nthy-ori 3-1 derivates for the modeling of the NRAS^{Q61R}-induced oncogenic transformation (upper panel); a workflow of the DISER (2D-**DI**GE + **SER**PA) technique (lower panel). B, Class stratification of candidate biomarkers according to the pattern of NRAS^{Q61R}-mediated regulation *in vitro* (upper right) and serological autoantibody reactivity observed in healthy volunteers (upper left) and in patients with NRAS^{Q61R} (lower right) or NRAS^{WT} (lower left) EFP/RLP tumors. 2D-DIGE – 2-dimensional difference gel electrophoresis; DISER, 2D-DIGE + SERPA; EFP/RLP, encapsulated follicular-patterned/RAS-like phenotype; SERPA, serological proteome analysis.

further visualized using Ponceau S staining for unlabeled proteins or fluorescent imaging for cyanine-labeled proteins as described below. Membranes were blocked and hybridized with individual patients' sera in a 1/500 dilution, with further workflow identical to that described in Ref. [16].

2.4. Image acquisition and analysis

The fluorescence of gels and membranes was detected using a Typhoon™ FLA 9500 laser scanner (GE Healthcare Life Sciences) at 50 μm/pixel resolution. For differential proteomic analysis, the Delta2D software program (DECODON GmbH) was used. Six representative gels were selected to ensure exhaustive dye swapping (see Supplementary Methods). Inter-gel warping was performed using automatic spot matching with further manual correction. The images were fused with a «Max Intensity» algorithm to generate a master gel, and spot detection and quantification were performed automatically.

Following enhanced chemiluminescent signal visualization, X-ray films exposed to blots for 15, 30, 60, and 120 s were scanned at 300 pixels/inch resolution without image enhancement; the overexposed (typically 120 s) films were used for precise manual positioning onto Ponceau S-stained or fluorescent membranes using the Adobe Photoshop software program, with further implicit positioning of short exposure films (15–30 s), which were used for subsequent analysis.

The fluorescent images of the membranes and gels were preprocessed using the ImageJ software program (Fiji distribution, https://imagej.net/Fiji/Downloads) to perform background removal, image equalization, unsharp masking, channel merge, and pseudo-coloring. A representative preprocessed gel image was selected and used as a target image for elastic registration of all membrane images using the bUnwarpJ plugin [20], and the transformation vectors for all individual registrations were used for identical transformations of matched prior positioned WB images. All registered images were then compiled into a single multi-layered file in Adobe Photoshop, which was visually inspected to identify protein spots demonstrating differential autoantibody reactivity between the studied groups.

2.5. Protein identification

The spots of interest were manually excised from CCBB-stained gels and subjected to in-gel digestion with trypsin. The resultant digests were applied to an Ultimate 3000 RSLCnano liquid chromatography system (Thermo Scientific) coupled with an Orbitrap Fusion mass spectrometer (Thermo Scientific). The tryptic digestion and LC-MS/MS analysis were performed similarly to those described in Ref. [21] with modifications (see Supplementary Methods). The raw files were converted to MASCOT generic format (.mgf), and the peak lists were obtained using OMSSA version 2.1.9 [22] via SearchGUI version 3.3.3 [23]. The protein identification was conducted against a concatenated target/decoy version of the *Homo sapiens* complement of the UniProtKB

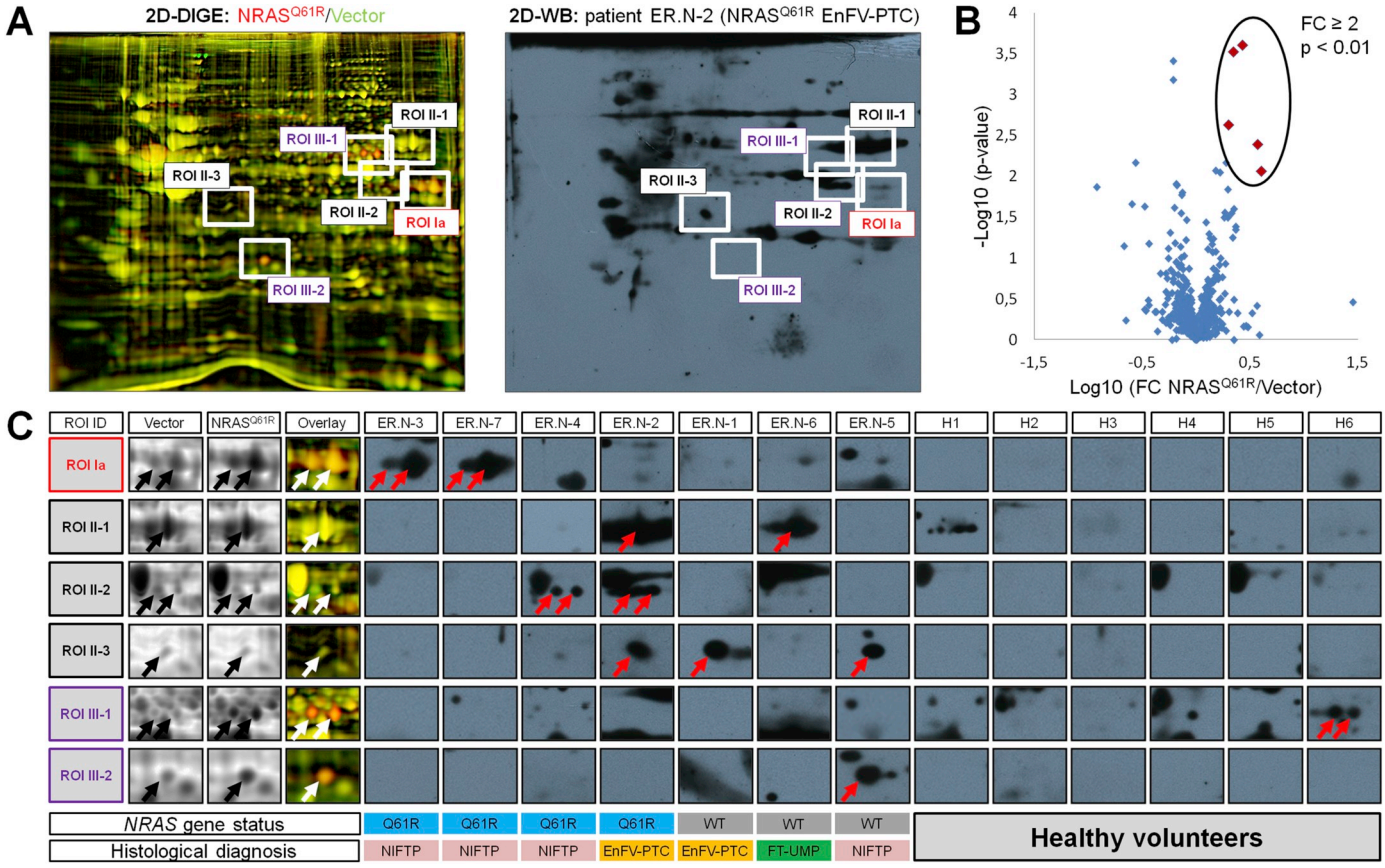

Fig. 2. Results of DISER profiling. A, Pseudo-colored merged channel image of a representative 2D-DIGE experiment (Nthy-ori 3-1-NRAS^{Q61R} proteins in red, Nthy-ori 3-1-Vector proteins in green) (left panel); representative 2D-WB hybridization pattern of EFP/RLP serum (patient ER.N-2, serum dilution 1/500) (right panel); ROIs corresponding to identified biomarker candidates are marked with rectangles. B, Volcano plot representing results of the quantitative analysis of proteomic differences between Nthy-ori 3-1-NRAS^{Q61R} and Nthy-ori 3-1-Vector cells inferred from six independent 2D-DIGE gels; class Ia and class III candidates are marked with the ellipse. C, Close-up sections of a representative 2D-DIGE image (Fig. 2A) and 2D-WB hybridization patterns demonstrated by EFP/RLP sera (dilution 1/500), corresponding to ROIs containing candidate biomarker spots (arrows); the lower panel depicts the *NRAS* gene status of EFP/RLP tumors along with corresponding pathological diagnoses. 2D-DIGE, 2-dimensional difference gel electrophoresis; 2D-WB, 2-dimensional Western blot analysis; DISER, 2D-DIGE + SERPA; EnFV-PTC, encapsulated follicular variant of papillary thyroid carcinoma; EFP/RLP, encapsulated follicular-patterned/RAS-like phenotype; FC, fold change; FT-UMP, follicular tumor of uncertain malignant potential; NIFTP, non-invasive follicular thyroid neoplasm with papillary-like nuclear features; ROI, region of interest.

Table 1
Results of 2D-DIGE analysis and MS/MS identification of the candidate biomarker proteins.

Spot ID[a]	2D-DIGE fold change ($NRAS^{Q61R}$/Vector)	2D-DIGE T-test p-value	Highest-ranked hit(s) gene name (emPAI[b])	Protein name	Theoretical pI/Mw (kDa)[c]	Sequence coverage (actual/possible[d])	Validated peptides
ROI Ia-alk	**2.22**	< **0.01**	PGK1 (2.78)	Phosphoglycerate kinase 1	8.30/44.5	67.39/100.00	30
ROI Ia-ac	**2.00**	< **0.01**	PGK1 (2.61)	Phosphoglycerate kinase 1	8.30/44.5	71.46/94.00	29
ROI II-1	1.04	NS[e]	PKM (0.81)	Pyruvate kinase PKM	7.95/57.8	36.53/94.16	16
ROI II-2-alk	0.88	NS	FH (0.40)	Fumarate hydratase, mitochondrial	6.99/50.1	21.96/91.57	7
ROI II-2-ac	0.62	NS	FH (0.21)	Fumarate hydratase, mitochondrial	6.99/50.1	8.63/91.57	4
ROI II-3	1.07	NS	CNN3 (1.74)	Calponin-3	5.69/36.4	39.82/73.86	14
			IDH3A (1.03)	Isocitrate dehydrogenase [NAD] subunit alpha, mitochondrial	5.71/36.6	33.61/66.39	12
ROI III-1-alk	**4.07**	< **0.01**	NAMPT (1.05)	Nicotinamide phosphoribosyltransferase	6.69/55.5	43.18/85.95	19
			GLUD1 (0.94)	Glutamate dehydrogenase 1, mitochondrial	6.71/56.0	36.38/79.93	19
			RTCB (0.61)	tRNA-splicing ligase RtcB homolog	6.77/55.2	27.33/70.30	12
ROI III-1-ac	**3.76**	< **0.01**	NAMPT (0.90)	Nicotinamide phosphoribosyltransferase	6.69/55.5	36.46/92.06	16
ROI III-2	**2.71**	< **0.01**	GSTO1 (1.37)	Glutathione S-transferase omega-1	6.23/27.4	41.91/85.89	12

[a] In ROI (regions of interest) containing two spots, postfix –alk was assigned to the more **alk**aline spot (right on all images) and postfix –ac to more **ac**idic spot (left on all images).

[b] Exponentially modified protein abundance index, calculated as $10^{\frac{N_{observed\ peptides}}{N_{observable\ peptides}}} - 1$ [25].

[c] For mitochondrial proteins, theoretical pI/Mw values correspond to mature forms lacking transit peptides.

[d] Actual coverage refers to a coverage value inferred from all peptides assigned to a given protein item and validated at 1% false discovery rate; possible coverage refers to maximal coverage that might be obtained if all peptides identifiable under defined search criteria were detected and validated.

[e] Not significant.

(version 1.9.2018, 20 373 target sequences), with the decoy sequences created by reversing the target sequences in SearchGUI. The identification settings were as follows: specific enzymatic digestion with trypsin, allowing up to 2 missed cleavages; b/y fragment ion type; MS^1 tolerance 10.0 ppm, MS^2 tolerance 0.01 Da; carbamidomethylation of C, acetylation of K, deamidation of Q, oxidation of M and phosphorylation of S, T, and Y were set as variable modifications. Peptides and proteins were inferred from the spectrum identification results using PeptideShaker version 1.16.26 [24]. Peptide spectrum matches, peptides, and proteins were validated at a 1% false discovery rate estimated using the decoy hit distribution. The lists of validated proteins were manually filtered to remove hits identified with a single validated peptide, as well as epidermal keratins and other possible contaminants. The remaining proteins were arranged in descending order of exponentially modified protein abundance index (emPAI) values [25], and the top-ranked hit together with those having emPAI > 0.5·emPAI (top-ranked hit) were referred to as the highest ranked.

2.6. Statistical analysis

The significance of between-group differences in autoantibody frequencies was tested using Fisher's exact test (http://www.quantitativeskills.com/sisa/statistics/fisher.htm). The significance of protein expression difference was tested using the Delta2D software-integrated statistical module utilizing the Student's T-test with the permutation-based calculation of the p-values and the Welch correction for unequal variances. The confidence intervals for proportions were calculated using a web-based calculator vassarstats.net/prop1.html.

3. Results

3.1. Establishment of the experimental system for studying the $NRAS^{Q61R}$ oncogene-induced immunome of thyroid follicular epithelia using the hybrid 2D-PAGE-based technique *DISER*

To model the $NRAS^{Q61R}$-induced oncogenic transformation, we utilized the cell system represented by Nthy-ori 3–1 cells that were stably transduced with $NRAS^{Q61R}$-encoding lentiviral construct (Fig. 1A) and demonstrated a cancer-like phenotype characterized by aberrant cellular morphology, increased anchorage-independent growth, hyperphosphorylated extracellular signal-regulated kinase (ERK), and an altered gene expression profile consistent with activation of the epithelial-mesenchymal transition (EMT) program [18]. We then established the analytical system for concurrent analysis of proteomic changes in Nthy-ori 3–1 cells in response to the expression of the EFP/RLP prototype driver $NRAS^{Q61R}$ and the autoantibody reactivity of the sera from EFP/RLP tumor patients against proteins expressed in Nthy-ori 3-1-$NRAS^{Q61R}$ cells. We utilized two gel-based proteomic techniques, 2D-DIGE and SERPA, and combined these into an experimental pipeline which we named **DISER** (Fig. 1A), where each experimental unit consisted of a 2D-DIGE using the proteins isolated from Nthy-ori 3-1-Vector and Nthy-ori 3-1-$NRAS^{Q61R}$ cells and individually labeled with different cyanine dyes, followed by electroblotting and WB hybridization with individual serum of a patient (Fig. 2A) or healthy volunteer

The candidate biomarkers identified by the **DISER** approach were stratified into four different classes as depicted in Fig. 1B. **Class Ia** biomarkers were of primary interest in our study, representing the oncogene-induced TAAs. **Class Ib** was assigned for less promising oncogene-induced TAAs with discordant patterns of autoantibody reactivity and *NRAS* mutation status of EFP/RLP tumors in autoantibody-positive patients. **Class II** biomarkers represented a group of TAAs whose expression was not influenced by oncogene expression. Finally, **class III** was reserved for candidate cell-based biomarkers with no or little relevance to the anti-tumor autoantibody response.

3.2. Concurrent identification of candidate cell-based and autoantibody biomarkers in EFP/RLP tumors using the ***DISER*** technique

We first analyzed the proteomic differences between Nthy-ori 3-1-NRAS^{Q61R} and Nthy-ori 3-1-Vector cells with special reference to the proteins overexpressed in response to oncogene expression. Out of 903 spots detected on the master gel containing protein features from 6 individual 2D-DIGE experiments, 5 spots demonstrated ≥2-fold upregulation at α-level 0.01 in Nthy-ori 3-1-NRAS^{Q61R} compared to Nthy-ori 3-1-Vector cells (Fig. 2B and Table 1). In SERPA profiling (Fig. 2C), two such spots within one region of interest (ROI) demonstrated recurrent strong autoantibody reactivity in the patients' group and no reactivity in the healthy volunteers' group, and thus were assigned to class Ia (two spots in ROI Ia), whereas the other NRAS^{Q61R}-induced proteins were assigned to class III (two spots in ROI III-1 and one spot in ROI III-2) as described above (Fig. 1B).

We then focused on proteins that did not demonstrate overexpression in response to NRAS^{Q61R} but that still might be of diagnostic value owing to recurrent strong specific autoantibody reactivity in tumor patients but not in healthy volunteers (class II as described above, Fig. 1B). The comparative analysis of 2D-WB hybridization patterns obtained from thirteen sera samples revealed four protein spots in three ROIs strongly and recurrently reactive in tumor patients but not in any of the six healthy volunteers' sera (one spot in ROI II-1, two spots in ROI II-2, and one spot in ROI II-3, Fig. 2C).

The protein content of the identified spots was then determined using the tandem mass spectrometry (MS/MS) analysis of the respective tryptic digests (Table 1). In the spot ROI III-1-alk, the three highest-ranked proteins were identified. However, only NAMPT and GLUD1 but not RTCB mRNA were found to be upregulated with fold change ≥2 in Nthy-ori 3-1-NRAS^{Q61R} compared to Nthy-ori 3-1-Vector cells (Supplementary Table 3). Similarly, the two highest-ranked proteins were identified in spot ROI II-3; however, the respective autoantibody reactivity pattern was recapitulated specifically by recombinant CNN3 (Supplementary Fig. 1). Taken together, the class Ia candidate was identified as PGK1; class II candidates as PKM, FH, and CNN3; and class III candidates as NAMPT, GLUD1, and GSTO1.

3.3. Meta-profiling of class I and II antigens' serological reactivity in thyroid neoplasia across the independent immunoproteomic experimental series

We then aimed to verify our findings in the extended sample of patients with various thyroid neoplasms. We have previously performed the classic SERPA profiling of serum autoantibody reactivity against proteins isolated from thyroid cancer cell lines K1 (papillary thyroid carcinoma) and follicular thyroid carcinoma (FTC-133) in three independent sample sets obtained from patients with the classic type of PTC (cPTC, non-EFP/RLP) and various EFP/RLP tumors (unpublished data) (Supplementary Table 2, validation sets 1–3). In the present study, we first used comparative 2D-DIGE to ensure that the spots corresponding to PGK1, PKM, and FH proteins were easily identifiable with high local abundance on the 2D maps of all three cell lines, thus allowing the direct cross-cell line comparison of 2D-WB hybridization patterns (Supplementary Fig. 2). Because the two highest-ranked proteins were identified in spot ROI II-3 (Table 1), the CNN3 autoantibody reactivities in the same sample sets were evaluated using recombinant CNN3 (see Supplementary Methods). We finally included yet another independent validation cohort (Supplementary Table 2, validation sets 4) to end up with a total of 20 cases of healthy controls, 19 cases of cPTC, and 41 cases of EFP/RLP tumors with different malignant potential (Fig. 3A) analyzed in a total of five independent experimental series including the discovery set (Supplementary Table 2).

All four antigens tested demonstrated recurrent strong autoantibody reactivity in patients with various thyroid neoplasms but not in the

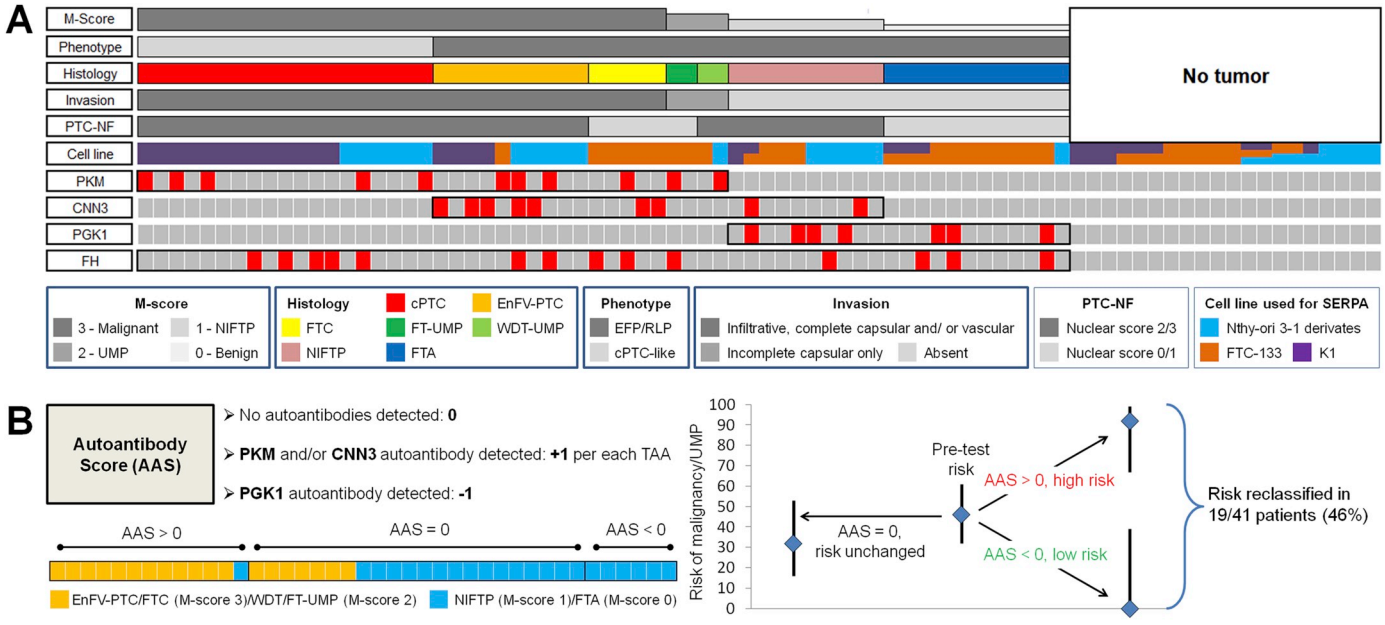

Fig. 3. Meta-profiling of serum autoantibody reactivity against class I and II candidates across five independent SERPA experimental series. A, The serological reactivity of identified antigens across various thyroid tumor groups; each column represents a single patient; strong autoantibody reactivities against individual antigens are marked with red rectangles. Also depicted are the key pathological features of individual tumors (see Supplementary Table 1 for the relevant descriptions), as well as the names of the cell lines used to obtain the 2D-WB hybridization patterns of individual sera. B, A prototype strategy for malignant/UMP tumor risk reclassification in EFP/RLP tumor patients using combined autoantibody score (AAS); calculation of AAS (upper left panel); distributions of malignant/UMP and NIFTP/FTA diagnoses in EFP/RLP tumors stratified according to AAS values (lower left panel); pre-test and reclassified using AAS malignancy/UMP risk estimates, depicted are point values along with 95% confidence intervals. AAS, autoantibody score; cPTC, classical type of papillary thyroid carcinoma; EFP/RLP, encapsulated follicular-patterned/RAS-like phenotype; EnFV-PTC, encapsulated follicular variant of papillary thyroid carcinoma; FTA, follicular thyroid adenoma; FTC, follicular thyroid carcinoma; FT-UMP, follicular tumor of uncertain malignant potential; NIFTP, non-invasive follicular thyroid neoplasm with papillary-like nuclear features; PTC-NF, nuclear features of papillary thyroid carcinoma; WDT-UMP, well-differentiated tumor of uncertain malignant potential.

healthy volunteers' group (Fig. 3A). As expected from the $NRAS^{Q61R}$-centered discovery setting (Fig. 1), none of identified TAA demonstrated a specific partitioning of the cognate autoantibodies' reactivities into the group of cPTC (Fig. 3A), the phenotype tightly associated with RAS-exclusive drivers $BRAF^{V600E}$ and RET/PTC [6,9]. FH autoantibodies were present in all groups of thyroid tumor patients (14/60 (23%) patients vs 0/20 control group; p = 0.016) without partitioning to any specific subgroup (Fig. 3A and Supplementary Fig. 3). PGK1 and CNN3 autoantibodies were present exclusively in patients with EFP/RLP tumors, with PGK1 autoantibodies only present in non-invasive lesions (M-score 0–1 EFP/RLP tumors: 7/22 (32%) vs 0/20 control group, p = 0.0092; 0/38 other tumors, p = 0.00044), and CNN3 autoantibodies specific to malignant and borderline lesions (M-score 1–3 EFP/RLP tumors: 9/29 (31%) vs 0/20 control group, p = 0.0067; 0/31 other tumors, p = 0.00068) (Fig. 3A and Supplementary Fig. 3). PKM autoantibodies were exclusively present in overtly malignant lesions and UMP tumors with incomplete capsular invasion without any association with the histological phenotype (M-score 2–3: 11/38 (29%) vs 0/20 control group, p = 0.011; 0/22 other tumors, p = 0.0046) (Fig. 3A and Supplementary Fig. 3). Upon limiting the analysis to EFP/RLP tumors (typically yielding the «indeterminate» FNAB cytology, i.e. Bethesda categories III, IV and V [13], Supplementary Table 2) and TAAs differentially reactive between tumors with different malignant potential (i.e. PKM, CNN3 and PGK1), the combined autoantibody score (AAS) allowed the reclassification of the pre-test risk of malignant/uncertain malignant potential (UMP) tumors in 19/41 (46%) of EFP/RLP tumor patients (Fig. 3B).

4. Discussion

The identification of disease-relevant candidates is a common challenge in immunoproteomics that has been successfully accomplished by other research groups via the implementation of specific non-genetic stimuli/events in cell systems used for autoantibody profiling [26,27]. Here, using the expression of oncogenic $NRAS^{Q61R}$ in Nthy-ori 3–1 cells and utilizing a multi-dimensional **DISER** approach (Fig. 1A), we identified a number of candidate cell-based and autoantibody biomarkers (Fig. 2 and Table 1) corresponding to classes III, II, and Ia as defined in Fig. 1B. Furthermore, we validated the two latter groups using the meta-profiling of the cognate autoantibodies' reactivities across an independent SERPA experimental series (Fig. 3A) and demonstrated the capability of the combined autoantibody score (AAS) to reclassify the pre-test risk of malignant/UMP tumors in EFP/RLP tumor patients (Fig. 3B).

The class III biomarkers (Fig. 1B) were identified from the 2D-DIGE module only (Fig. 1A) as candidate cell-based biomarkers that were specifically upregulated by $NRAS^{Q61R}$ (Fig. 2, ROIs III-1 and III-2) with no, non-recurrent or contextually irrelevant patterns of autoantibody reactivity (Fig. 2C). The identified class III candidates (NAMPT, GLUD1, and GSTO1, Table 1) were implicated in human cancer, including thyroid carcinomas [28,29], and were shown to operate a variety of pathways that contributed to tumor metabolism [30,31] drug resistance [32–34], and the stemness of cancer cells [35,36]. All three class III candidates are currently considered to be potential targets for cancer therapy [37–39], and our data provide some preliminary *in vitro* basis for the appropriate selection of tumor genotypes that would most likely respond to such treatment.

The class II biomarkers (Fig. 1B) were defined as candidate TAAs that were identified from the SERPA module only (Fig. 1A), with no apparent evidence of $NRAS^{Q61R}$-mediated regulation (Fig. 2, ROIs II-1, II-2, and II-3). All identified class II candidates (Table 1) were implicated in human cancer to a varying degree (see below), with mutations in the fumarate hydratase (*FH*) gene being the most notable for its role in the development of autosomal dominant hereditary leiomyomatosis and renal cell carcinoma (HLRCC) syndrome (reviewed in Ref. [40]).

In the human thyroid, FH has recently been identified as being the top 5th protein upregulated in follicular carcinomas compared to follicular adenomas [41]; however, in our experiments, this pattern was not replicated by the FH autoantibody, with the latter encountered in all types of thyroid neoplasia (Fig. 3A). Notwithstanding, it still may be potentially used for the discrimination of neoplastic from non-neoplastic thyroid disease because no FH autoantibody reactivity was detected in healthy volunteers (Figs. 2C and 3A and Supplementary Fig. 3).

Another class II antigen with a more restricted pattern of autoantibody reactivity (i.e. specific to malignant and borderline EFP/RLP tumors, Fig. 3A) was identified as a thin filament-associated protein calponin-3 (CNN3) (Table 1). Unlike its well-studied smooth muscle-specific homolog CNN1, the functions of non-muscle CNN3 have been documented rather poorly, yet it was implicated in stress fiber formation and contractility [42,43] and cell migration [44]. In gastrointestinal neoplasms, CNN3 was implicated in cell invasion, chemoresistance, and EMT, as well as in lymph node and peritoneal seeding metastases [45–49]. Given the critical role or RAS/RAF/MAPK signaling in molecular pathogenesis of thyroid tumors (reviewed in Ref. [50]), the reported implication of CNN3 in the activation ERK1/2 in REF52.2 fibroblasts [44] is of interest, although the relevance of these findings to human tumors and thyroid cancer in particular is unclear.

In the human thyroid, the CNN3 mRNA was found to be upregulated in the follicular variant of PTC compared to cPTC [51], which is in agreement with our data on the presence of CNN3 autoantibodies in EFP/RLP tumors but not in cPTC (Fig. 3A). At the same time, we observed neither specificity of CNN3 autoantibodies to NRAS-mutant tumors (Fig. 2C) nor any overexpression of CNN3 protein in Nthy-ori 3-1-$NRAS^{Q61R}$ compared to Nthy-ori 3-1-Vector cells (Fig. 2C and Table 1). However, significant upregulation of CNN3 mRNA was previously demonstrated upon the expression of another mutant RAS oncogene $HRAS^{G12V}$ in transformed ovarian epithelia [52]. These data suggest that drivers different from $NRAS^{Q61R}$ but still associated with RAS-like phenotype may contribute to the CNN3 overexpression and/or autoantibody reactivity in EFP/RLP tumors.

The final, and probably the most promising, class II candidate, was identified as a glycolytic enzyme pyruvate kinase PKM (Table 1), catalyzing the final and the second ATP-generating step in the glycolytic pathway. The PKM2 splice isoform is the predominant PKM variant found in high-proliferating normal and cancer tissues that has been widely implicated as one of the central mediators of the Warburg effect and in acquiring of the malignant phenotype [53–55]. For a long time, it has been widely believed that PKM1→PKM2 isoform shift primarily accounts for the elevated levels of PKM2 in cancer tissues, although this view was repeatedly challenged [56–58]. Nevertheless, the overexpression of PKM does occur in the majority of human cancers [57,58], and the high level of PKM2 is associated with poor prognosis in most solid malignancies [59]. This is also the case for thyroid carcinomas, where PKM2 overexpression is reportedly associated with $BRAF^{V600E}$ mutation and aggressive tumor features [60]. The tumor-promoting functions of PKM2 in thyroid carcinogenesis were repeatedly demonstrated using siRNA-mediated knockdown and/or overexpression of PKM2 both *in vitro* in thyroid cancer cell lines and *in vivo* using mouse xenografts, and the role of the down-regulation of tumor-suppressive microRNAs miR-148a and miR-326 in the overexpression of PKM2 was also established [60,61].

Taking into account the positive influence of PKM2 on the migratory and invasive characteristics of thyroid cancer cells [60,61], PKM overexpression is likely to represent a hallmark of a fully malignant phenotype in thyroid neoplasia. By contrast, the RAS mutations are comparably prevalent in benign, malignant and borderline EFP/RLP tumors [4–12], thus representing an early event in thyroid carcinogenesis [62]. Indeed, PKM protein was not upregulated in Nthy-ori 3-1-$NRAS^{Q61R}$ cells compared to Nthy-ori 3-1-Vector cells (Fig. 2C and Table 1), whereas PKM autoantibodies were observed exclusively in

patients with overtly malignant lesions (belonging both to the cPTC and the EFP/RLP phenotypes) and UMP tumors with incomplete capsular invasion (Figs. 2C and 3A). These results implicate PKM autoantibody as a histological phenotype-independent biomarker of malignancy in thyroid neoplasia.

The class Ia biomarkers (Fig. 1B) that demonstrated both autoantibody reactivity in EFP/RLP tumors and protein upregulation in response to $NRAS^{Q61R}$ expression (Fig. 2, ROI Ia) were of primary interest in our study, and such a candidate was identified as another glycolytic enzyme phosphoglycerate kinase PGK1 (Table 1). In the glycolytic pathway, PGK1 alongside with PKM (described above) are the only ATP-generating enzymes; the identification of both of these proteins as thyroid neoplasia-associated TAA is rather intriguing, particularly provided that the tumor subgroup partitioning patterns of the cognate autoantibodies appear to be mutually exclusive (Figs. 2C and 3A).

The overexpression of PGK1 was reported in human cancer and implicated in promoting tumor progression, metastases, angiogenesis and drug resistance [63–69]. Recently, the novel activity of PGK1 as a tumor-promoting protein kinase was discovered, implicating PGK1 as a crucial coordinator of multiple oncogenic pathways. Under glutamine deprivation or hypoxia stimulation, PGK1 was acetylated at K388 by acetyl-transferase ARD1; the acetylated PGK1 then bound to and phosphorylated Beclin-1 (BCLN1) to ultimately promote the initiation of autophagy. In another model, hypoxia, activation of EGFR signaling and, importantly, the expression of oncogenic $BRAF^{V600E}$ or $KRAS^{G12V}$ resulted in ERK-dependent phosphorylation of PGK1 at S203 with subsequent PIN1-dependent *cis-trans* isomerization at pS203P204, triggering PGK1 conformational changes with exposure of the mitochondrial targeting signal. The mitochondria-localized PGK1 then phosphorylated pyruvate dehydrogenase kinase 1 (PDHK1) to coordinate glycolysis and the tricarboxylic acid cycle. In both of these studies, the PGK1-dependent phosphorylation of the relevant substrates promoted brain tumorigenesis in athymic nude mice and was associated with poor survival in glioblastoma patients [70,71].

In line with our data (Fig. 2C and Table 1), upregulation of PGK1 was also observed upon the expression of oncogenic $HRAS^{G12V}$ in transformed NIH 3T3 mouse fibroblasts [72]. Moreover, high PGK1 levels were found in follicular adenomas and in follicular variant of PTC but not in cPTC lesions, implicating PGK1 as a potential biomarker for discriminating between cPTC and EFP/RLP tumors [73,74]. The meta-profiling of PGK1 autoantibody reactivity also demonstrated specificity towards EFP/RLP tumors (Fig. 3A), implicating PGK1 overexpression induced by mutant RAS (and probably by other drivers associated with RAS-like phenotype) as a possible immunogenic stimulus pertinent to PGK1 autoantibody production. Interestingly, further restriction of PGK1 autoantibodies to benign/non-invasive lesions (Fig. 3A) implicates PGK1 autoantibody as a potential biomarker for discriminating between EFP/RLP lesions with different malignant potential. However, provided the association of high PGK1 levels with highly malignant phenotype in other human tumors [63–69], the observed pattern is somewhat unexpected and warrants further investigation.

Of note, both neoplasms that were found to be associated with PGK1 autoantibodies (pancreatic carcinoma [75] and thyroid EFP/RLP tumors in the present study) are among the tumors that are most highly dependent on mutationally activated RAS signaling [4–12,76], and at the same time express high levels of PGK1 [65,73,74]. These data further stress the possible interconnection between the activation of RAS cascade, PGK1 overexpression, and PGK1 autoantibody production. Moreover, provided the abovementioned data on the non-classical functions and subcellular localization of PGK1 upon $KRAS^{G12V}$ expression [70], it would be intriguing to speculate that mutant RAS-dependent post-translational modifications, structural changes, and/or mitochondrial translocation of PGK1 might act concurrently with PGK1 overexpression as immunogenic stimuli triggering an autoantibody response in these neoplasms. This hypothetical model warrants further study in the future.

Similarly to the majority of TAAs identified to date (reviewed in Ref. [1]), the autoantibodies targeting class I and II TAAs identified in our study (with the exception of CNN3) have also been described in other human cancers, such as PGK1 in pancreatic carcinoma [75], PKM in oral cavity [77] and breast [78] carcinomas, and FH in lung [79] and hepatocellular [80] carcinomas, as well as in melanomas [81]. This implies that the mechanisms underlying the cancer-associated immunogenicity of these proteins may be shared with other cancer types and oncogenic pathways. Although this somewhat compromises the specificity of identified biomarkers to thyroid carcinoma, there are only a few clinical scenarios where it might be important (e.g., independently evolved synchronous cancer in other organs, metastatic cancer of unknown primary site), which all represent rare and complicated situations warranting specifically dedicated settings of biomarker discovery.

Similarly and characteristically of most known TAAs, all class I and II candidates identified in our study demonstrated very high diagnostic specificity, but relatively low diagnostic sensitivity in the detection of a particular tumor phenotype (see paragraph 3.3 and Supplementary Fig. 3). This implies that the real clinical use of identified biomarkers might require combination thereof with each other and/or other autoantibodies or other types of biomarkers. Upon incorporation of the three autoantibodies differentially reactive between the groups of tumors with different malignant potential (i.e. PKM, CNN3 and PGK1 autoantibodies, Fig. 3A) to yield the combined autoantibody score (AAS), nearly half of EFP/RLP tumor patients had their malignant/UMP tumor risk reclassified as compared to the pre-test value (Fig. 3B). Although this data from a small highly selected cohort should be interpreted with significant caution and need to be confirmed in a fully prospective setting, we believe that such an algorithm may aid the treatment decisions in a significant proportion of patients with «indeterminate» FNAB cytology (i.e. Bethesda categories III, IV, and V [13]).

Taken together, here we demonstrated that *in vitro* oncogene expression coupled with the **DISER** technique combines and improves the advantages of the 2D-DIGE and SERPA methods, allowing the concurrent identification of candidate cell-based and autoantibody biomarkers, and further provides an analytical filter to focus the search strategy on the oncogene-induced TAAs. Using this approach, we identified a number of candidate cell-based and circulating autoantibody biomarkers. Provided the establishment of clinically applicable straightforward assays (e.g. conventional enzyme-linked immunosorbent assay, Luminex xMAP technology etc.), these autoantibodies may be potentially suitable for identifying of the neoplastic nature of thyroid nodule (FH), identification of malignant/UMP tumors (PKM), and discriminating between EFP/RLP lesions with different malignant potential (CNN3 and $NRAS^{Q61R}$-induced TAA PGK1). Further research on $BRAF^{V600E}$ and RET/PTC1 utilizing the **DISER** approach is underway to identify additional autoantigens that might be associated with these RAS-exclusive drivers and thus expand the list of potential autoantibody biomarkers of thyroid neoplasia beyond those associated with EFP/RLP tumors identified in the current and previous [16] studies.

Although in our study the **DISER** approach was implemented in conjunction with *in vitro* oncogene expression, this technique may be employed in a wider variety of experimental settings, e.g., profiling of primary tumors/matched normal tissue pairs with autologous sera, which may be capable of further identifying highly immunogenic neoantigens resulting from frameshift or splice site mutations. Cellular compartment-targeted proteomics or other types of prefractionation (reviewed in Ref. [82]) may aid in the identification of additional low-abundance autoantigens, while simultaneous recapitulation of several oncogenic events in appropriate immortalized non-tumorous cell lines might allow the modeling of more genetically complex neoplasms and the identification of disease-relevant autoantigens regulated by concurrent action of multiple oncogenic pathways.

Funding

The majority of work was supported by the Russian Science Foundation (project # 16-15-10423). The sample collection and pathological workup (Supplementary Table 2) was in part supported by the Ministry of Education and Science of the Russian Federation (project # 02.A03.21.0004).

Conflicts of interest

The authors declare that they have no potential conflicts of interest.

Acknowledgments

We would like to thank Dr. Kristoffer Riecken (Medical Center Hamburg-Eppendorf) for kindly providing the LeGO-iPuro2 lentiviral vector. We are grateful to Prof. Sergei Nedospasov, head of Department of Immunology (Biological Faculty, Lomonosov Moscow State University), for continuous support and helpful discussions. We are thankful to Mr. Georg Wrettos, application specialist in DECODON GmbH (Greifswald, Germany), for providing the Delta2D trial license and for his helpful discussions on Delta2D functionality and statistical analysis. We also greatly appreciate the work of the members of the International Pathology Panel of the Chernobyl Tissue Bank (CTB) and the scientific and technical staff of the Russian CTB repository at the Tsyb Medical Radiological Research Center (Obninsk, Russia).

Appendix A. Supplementary data

Supplementary data to this article can be found online at https://doi.org/10.1016/j.canlet.2019.07.013.

References

[1] J. Wu, X. Li, W. Song, Y. Fang, L. Yu, S. Liu, L.P. Churilov, F. Zhang, The roles and applications of autoantibodies in progression, diagnosis, treatment and prognosis of human malignant tumours, Autoimmun. Rev. 16 (2017) 1270–1281, https://doi.org/10.1016/j.autrev.2017.10.012.

[2] M. Zoccarato, M. Gastaldi, L. Zuliani, T. Biagioli, M. Brogi, G. Bernardi, E. Corsini, E. Bazzigaluppi, R. Fazio, C. Giannotta, E. Nobile-Orazio, G. Costa, R. Iorio, A. Evoli, S. Mariotto, S. Ferrari, E. Galloni, V. De Riva, E. Zardini, D. Franciotta, B. Giometto, Diagnostics of paraneoplastic neurological syndromes, Neurol. Sci. 38 (2017) 237–242, https://doi.org/10.1007/s10072-017-3031-5.

[3] W.C.G. van Staveren, D.Y.W. Solís, A. Hébrant, V. Detours, J.E. Dumont, C. Maenhaut, Human cancer cell lines: experimental models for cancer cells in situ? For cancer stem cells? Biochim. Biophys. Acta 1795 (2009) 92–103, https://doi.org/10.1016/j.bbcan.2008.12.004.

[4] M. Rivera, J. Ricarte-Filho, J. Knauf, A. Shaha, M. Tuttle, J.A. Fagin, R.A. Ghossein, Molecular genotyping of papillary thyroid carcinoma follicular variant according to its histological subtypes (encapsulated vs infiltrative) reveals distinct BRAF and RAS mutation patterns, Mod. Pathol. 23 (2010) 1191–1200, https://doi.org/10.1038/modpathol.2010.112.

[5] M. Fukahori, A. Yoshida, H. Hayashi, M. Yoshihara, S. Matsukuma, Y. Sakuma, S. Koizume, N. Okamoto, T. Kondo, M. Masuda, Y. Miyagi, The associations between RAS mutations and clinical characteristics in follicular thyroid tumors: new insights from a single center and a large patient cohort, Thyroid 22 (2012) 683–689, https://doi.org/10.1089/thy.2011.0261.

[6] S.-K. Yoo, S. Lee, S.-J. Kim, H.-G. Jee, B.-A. Kim, H. Cho, Y.S. Song, S.W. Cho, J.-K. Won, J.-Y. Shin, D.J. Park, J.-I. Kim, K.E. Lee, Y.J. Park, J.-S. Seo, Comprehensive analysis of the transcriptional and mutational landscape of follicular and papillary thyroid cancers, PLoS Genet. 12 (2016) e1006239, https://doi.org/10.1371/journal.pgen.1006239.

[7] S.-H. Jung, M.S. Kim, C.K. Jung, H.-C. Park, S.Y. Kim, J. Liu, J.-S. Bae, S.H. Lee, T.-M. Kim, S.H. Lee, Y.-J. Chung, Mutational burdens and evolutionary ages of thyroid follicular adenoma are comparable to those of follicular carcinoma, Oncotarget 7 (2016) 69638–69648, https://doi.org/10.18632/oncotarget.11922.

[8] C.K. Jung, Y. Kim, S. Jeon, K. Jo, S. Lee, J.S. Bae, Clinical utility of EZH1 mutations in the diagnosis of follicular-patterned thyroid tumors, Hum. Pathol. 81 (2018) 9–17, https://doi.org/10.1016/j.humpath.2018.04.018.

[9] The Cancer Genome Atlas Research Network, Integrated genomic characterization of papillary thyroid carcinoma, Cell 159 (2014) 676–690, https://doi.org/10.1016/j.cell.2014.09.050.

[10] Y.S. Song, J.-K. Won, S.-K. Yoo, K.C. Jung, M.J. Kim, S.-J. Kim, S.W. Cho, K.E. Lee, K.H. Yi, J.-S. Seo, Y.J. Park, Comprehensive transcriptomic and genomic profiling of subtypes of follicular variant of papillary thyroid carcinoma, Thyroid (2018), https://doi.org/10.1089/thy.2018.0198.

[11] U. Cho, O. Mete, M.-H. Kim, J.S. Bae, C.K. Jung, Molecular correlates and rate of lymph node metastasis of non-invasive follicular thyroid neoplasm with papillary-like nuclear features and invasive follicular variant papillary thyroid carcinoma: the impact of rigid criteria to distinguish non-invasive follicular thyroid neoplasm with papillary-like nuclear features, Mod. Pathol. 30 (2017) 810–825, https://doi.org/10.1038/modpathol.2017.9.

[12] Z. Liu, G. Zhou, M. Nakamura, E. Koike, Y. Li, T. Ozaki, I. Mori, E. Taniguchi, K. Kakudo, Encapsulated follicular thyroid tumor with equivocal nuclear changes, so-called well-differentiated tumor of uncertain malignant potential: a morphological, immunohistochemical, and molecular appraisal, Cancer Sci. 102 (2011) 288–294, https://doi.org/10.1111/j.1349-7006.2010.01769.x.

[13] E.S. Cibas, S.Z. Ali, The 2017 Bethesda system for reporting thyroid cytopathology, Thyroid 27 (2017) 1341–1346, https://doi.org/10.1089/thy.2017.0500.

[14] K. Ohlendieck (Ed.), Difference Gel Electrophoresis, Springer New York, New York, NY, 2018, https://doi.org/10.1007/978-1-4939-7268-5.

[15] C.S. Klade, T. Voss, E. Krystek, H. Ahorn, K. Zatloukal, K. Pummer, G.R. Adolf, Identification of tumor antigens in renal cell carcinoma by serological proteome analysis, Proteomics 1 (2001) 890–898, https://doi.org/10.1002/1615-9861(200107)1:7<890::AID-PROT890>3.0.CO;2-Z.

[16] P.V. Belousov, A.V. Bogolyubova, Y.S. Kim, A.Y. Abrosimov, A.T. Kopylov, A.A. Tvardovskiy, K.V. Lanshchakov, A.Y. Sazykin, N.Y. Dvinskikh, Y.I. Bobrovskaya, L.S. Selivanova, E.S. Shilov, A.M. Schwartz, Y.V. Shebzukhov, N.V. Severskaia, V.E. Vanushko, S.A. Moshkovskii, S.A. Nedospasov, D.V. Kuprash, Serum immunoproteomics combined with pathological reassessment of surgical specimens identifies TCP-1ζ autoantibody as a potential biomarker in thyroid neoplasia, J. Clin. Endocrinol. Metab. 100 (2015) E1206–E1215, https://doi.org/10.1210/jc.2014-4260.

[17] R.V. Lloyd, R.Y. Osamura, G. Klöppel, J. Rosai, World health organization., international agency for research on cancer., tumours of the thyroid gland, in: R.V. Lloyd, R.Y. Osamura, G. Klöppel, J. Rosai (Eds.), WHO Classif. Tumours Endocr. Organs, fourth ed., IARC Press, Lyon, 2017, pp. 81–92 2017.

[18] D.E. Demin, M.A. Afanasyeva, A.N. Uvarova, M.M. Prokofjeva, A.M. Gorbachova, A.S. Ustiugova, A.V. Klepikova, L.V. Putlyaeva, K.A. Tatosyan, P.V. Belousov, A.M. Schwartz, Constitutive expression of NRAS with Q61R driver mutation activates processes of epithelial–mesenchymal transition and leads to substantial transcriptome change of Nthy-ori 3–1 thyroid epithelial cells, Biochem 84 (2019) 416–425, https://doi.org/10.1134/S0006297919040096.

[19] K. Weber, U. Bartsch, C. Stocking, B. Fehse, A multicolor panel of novel lentiviral "gene ontology" (LeGO) vectors for functional gene analysis, Mol. Ther. 16 (2008) 698–706, https://doi.org/10.1038/mt.2008.6.

[20] C.O.S. Sorzano, I. Arganda-Carreras, P. Thévenaz, A. Beloso, G. Morales, I. Valdés, C. Pérez-García, C. Castillo, E. Garrido, M. Unser, Elastic image registration of 2-D gels for differential and repeatability studies, Proteomics 8 (2008) 62–65, https://doi.org/10.1002/pmic.200700473.

[21] M.A. Afanasyeva, A.S. Ustiugova, S.A. Golyshev, A.T. Kopylov, A.V. Bogolyubova, D.E. Demin, P.V. Belousov, A.M. Schwartz, Isolation of large amounts of highly pure mitochondria for "Omics" studies, Biochemistry. (Mosc). 83 (2018) 76–85, https://doi.org/10.1134/S0006297918010108.

[22] L.Y. Geer, S.P. Markey, J.A. Kowalak, L. Wagner, M. Xu, D.M. Maynard, X. Yang, W. Shi, S.H. Bryant, Open mass spectrometry search algorithm, J. Proteome Res. 3 (2004) 958–964, https://doi.org/10.1021/pr0499491.

[23] M. Vaudel, H. Barsnes, F.S. Berven, A. Sickmann, L. Martens, SearchGUI: an open-source graphical user interface for simultaneous OMSSA and X!Tandem searches, Proteomics 11 (2011) 996–999, https://doi.org/10.1002/pmic.201000595.

[24] M. Vaudel, J.M. Burkhart, R.P. Zahedi, E. Oveland, F.S. Berven, A. Sickmann, L. Martens, H. Barsnes, PeptideShaker enables reanalysis of MS-derived proteomics data sets, Nat. Biotechnol. 33 (2015) 22–24, https://doi.org/10.1038/nbt.3109.

[25] Y. Ishihama, Y. Oda, T. Tabata, T. Sato, T. Nagasu, J. Rappsilber, M. Mann, Exponentially modified protein abundance index (emPAI) for estimation of absolute protein amount in proteomics by the number of sequenced peptides per protein, Mol. Cell. Proteom. 4 (2005) 1265–1272, https://doi.org/10.1074/mcp.M500061-MCP200.

[26] T.R. Cottrell, J.C. Hall, A. Rosen, L. Casciola-Rosen, Identification of novel autoantigens by a triangulation approach, J. Immunol. Methods 385 (2012) 35–44, https://doi.org/10.1016/j.jim.2012.07.024.

[27] M. Grandjean, A. Sermeus, S. Branders, F. Defresne, M. Dieu, P. Dupont, M. Raes, M. De Ridder, O. Feron, Hypoxia integration in the serological proteome analysis unmasks tumor antigens and fosters the identification of anti-phospho-eEF2 antibodies as potential cancer biomarkers, PLoS One 8 (2013) e76508, https://doi.org/10.1371/journal.pone.0076508.

[28] H.M. Kim, Y.K. Lee, J.S. Koo, Expression of glutamine metabolism-related proteins in thyroid cancer, Oncotarget 7 (2016) 53628–53641, https://doi.org/10.18632/oncotarget.10682.

[29] N. Sawicka-Gutaj, J. Waligórska-Stachura, M. Andrusiewicz, M. Biczysko, J. Sowiński, J. Skrobisz, M. Ruchała, Nicotinamide phosphorybosiltransferase overexpression in thyroid malignancies and its correlation with tumor stage and with survivin/survivin DEx3 expression, Tumour Biol 36 (2015) 7859–7863, https://doi.org/10.1007/s13277-015-3506-z.

[30] H. Chen, S. Wang, H. Zhang, E.C. Nice, C. Huang, Nicotinamide phosphoribosyltransferase (Nampt) in carcinogenesis: new clinical opportunities, Expert Rev. Anticancer Ther. 16 (2016) 827–838, https://doi.org/10.1080/14737140.2016.1190649.

[31] A. Plaitakis, E. Kalef-Ezra, D. Kotzamani, I. Zaganas, C. Spanaki, The glutamate dehydrogenase pathway and its roles in cell and tissue biology in health and disease, Biology (Basel). 6 (2017) 11, https://doi.org/10.3390/biology6010011.

[32] X. Yan, L. Pan, Y. Yuan, J. Lang, N. Mao, Identification of platinum-resistance associated proteins through proteomic analysis of human ovarian cancer cells and their platinum-resistant sublines, J. Proteome Res. 6 (2007) 772–780, https://doi.org/10.1021/pr060402r.
[33] S. Piaggi, C. Raggi, A. Corti, E. Pitzalis, M.C. Mascherpa, M. Saviozzi, A. Pompella, A.F. Casini, Glutathione transferase omega 1-1 (GSTO1-1) plays an anti-apoptotic role in cell resistance to cisplatin toxicity, Carcinogenesis 31 (2010) 804–811, https://doi.org/10.1093/carcin/bgq031.
[34] M. Ohanna, M. Cerezo, N. Nottet, K. Bille, R. Didier, G. Beranger, B. Mograbi, S. Rocchi, L. Yvan-Charvet, R. Ballotti, C. Bertolotto, Pivotal role of NAMPT in the switch of melanoma cells toward an invasive and drug-resistant phenotype, Genes Dev. 32 (2018) 448–461, https://doi.org/10.1101/gad.305854.117.
[35] A. Lucena-Cacace, D. Otero-Albiol, M.P. Jiménez-García, J. Peinado-Serrano, A. Carnero, NAMPT overexpression induces cancer stemness and defines a novel tumor signature for glioma prognosis, Oncotarget 8 (2017) 99514–99530, https://doi.org/10.18632/oncotarget.20577.
[36] A. Lucena-Cacace, D. Otero-Albiol, M.P. Jiménez-García, S. Muñoz-Galvan, A. Carnero, NAMPT is a potent oncogene in colon cancer progression that modulates cancer stem cell properties and resistance to therapy through Sirt1 and PARP, Clin. Cancer Res. 24 (2018) 1202–1215, https://doi.org/10.1158/1078-0432.CCR-17-2575.
[37] D. Sampath, T.S. Zabka, D.L. Misner, T. O'Brien, P.S. Dragovich, Inhibition of nicotinamide phosphoribosyltransferase (NAMPT) as a therapeutic strategy in cancer, Pharmacol. Ther. 151 (2015) 16–31, https://doi.org/10.1016/j.pharmthera.2015.02.004.
[38] Y.-K. Choi, K.-G. Park, Targeting glutamine metabolism for cancer treatment, Biomol. Ther. (Seoul). 26 (2018) 19–28, https://doi.org/10.4062/biomolther.2017.178.
[39] K. Ramkumar, S. Samanta, A. Kyani, S. Yang, S. Tamura, E. Ziemke, J.A. Stuckey, S. Li, K. Chinnaswamy, H. Otake, B. Debnath, V. Yarovenko, J.S. Sebolt-Leopold, M. Ljungman, N. Neamati, Mechanistic evaluation and transcriptional signature of a glutathione S-transferase omega 1 inhibitor, Nat. Commun. 7 (2016) 13084, https://doi.org/10.1038/ncomms13084.
[40] S.L. Skala, S.M. Dhanasekaran, R. Mehra, Hereditary leiomyomatosis and renal cell carcinoma syndrome (HLRCC): a contemporary review and practical discussion of the differential diagnosis for HLRCC-associated renal cell carcinoma, Arch. Pathol. Lab Med. 142 (2018) 1202–1215, https://doi.org/10.5858/arpa.2018-0216-RA.
[41] X. Lai, C.B. Umbricht, K. Fisher, J. Bishop, Q. Shi, S. Chen, Identification of novel biomarker and therapeutic target candidates for diagnosis and treatment of follicular carcinoma, J. Proteomics. 166 (2017) 59–67, https://doi.org/10.1016/j.jprot.2017.07.003.
[42] E. Daimon, Y. Shibukawa, Y. Wada, Calponin 3 regulates stress fiber formation in dermal fibroblasts during wound healing, Arch. Dermatol. Res. 305 (2013) 571–584, https://doi.org/10.1007/s00403-013-1343-8.
[43] K. Ciuba, W. Hawkes, S. Tojkander, K. Kogan, U. Engel, T. Iskratsch, P. Lappalainen, Calponin-3 is critical for coordinated contractility of actin stress fibers, Sci. Rep. 8 (2018) 17670, https://doi.org/10.1038/s41598-018-35948-6.
[44] S. Appel, P.G. Allen, S. Vetterkind, J.-P. Jin, K.G. Morgan, h3/Acidic calponin: an actin-binding protein that controls extracellular signal-regulated kinase 1/2 activity in nonmuscle cells, Mol. Biol. Cell 21 (2010) 1409–1422, https://doi.org/10.1091/mbc.e09-06-0451.
[45] K.-S. Hong, H. Kim, S.-H. Kim, M. Kim, J. Yoo, Calponin 3 regulates cell invasion and doxorubicin resistance in gastric cancer, Gastroenterol. Res. Pract. 2019 (2019) 3024970, https://doi.org/10.1155/2019/3024970.
[46] C. Nakarai, K. Osawa, M. Akiyama, N. Matsubara, H. Ikeuchi, T. Yamano, S. Hirota, N. Tomita, M. Usami, Y. Kido, Expression of AKR1C3 and CNN3 as markers for detection of lymph node metastases in colorectal cancer, Clin. Exp. Med. 15 (2015) 333–341, https://doi.org/10.1007/s10238-014-0298-1.
[47] S.-C. Kim, C.-W. Hong, S.-G. Jang, Y.-A. Kim, B.-C. Yoo, Y.-K. Shin, S.-Y. Jeong, J.-L. Ku, J.-G. Park, Establishment and characterization of paired primary and peritoneal seeding human colorectal cancer cell lines: identification of genes that mediate metastatic potential, Transl. Oncol. 11 (2018) 1232–1243, https://doi.org/10.1016/j.tranon.2018.07.014.
[48] W. Abdel-Rahman, V. Nair, N. Al-khayyal, PO-206: Calponin 3 (CNN3) promotes epithelial to mesenchymal transition and drug resistance of colon cancer cells, ESMO Open 3 (2018), https://doi.org/10.1136/esmoopen-2018-EACR25.241.
[49] S.-C. Kim, C.-W. Hong, S.-G. Jang, Y.-A. Kim, S.-Y. Jung, J.-G. Park, J.-L. Ku, Abstract 1642: Calponin-3, acidic (CNN3) mediates EMT-related genes in human colorectal cancer metastasis, Cancer Res. 76 (14 Supplement) (2016) 1642, https://doi.org/10.1158/1538-7445.AM2016-1642.
[50] M.A. Zaballos, P. Santisteban, Key signaling pathways in thyroid cancer, J. Endocrinol. 235 (2017) R43–R61, https://doi.org/10.1530/JOE-17-0266.
[51] S. Chevillard, N. Ugolin, P. Vielh, K. Ory, C. Levalois, D. Elliott, G.L. Clayman, A.K. El-Naggar, Gene expression profiling of differentiated thyroid neoplasms: diagnostic and clinical implications, Clin. Cancer Res. 10 (2004) 6586–6597, https://doi.org/10.1158/1078-0432.CCR-04-0053.
[52] T. Young, F. Mei, J. Liu, R.C. Bast, A. Kurosky, X. Cheng, Proteomics analysis of H-RAS-mediated oncogenic transformation in a genetically defined human ovarian cancer model, Oncogene 24 (2005) 6174–6184, https://doi.org/10.1038/sj.onc.1208753.
[53] B. Chaneton, E. Gottlieb, Rocking cell metabolism: revised functions of the key glycolytic regulator PKM2 in cancer, Trends Biochem. Sci. 37 (2012) 309–316, https://doi.org/10.1016/j.tibs.2012.04.003.
[54] T.L. Dayton, T. Jacks, M.G. Vander Heiden, PKM2, cancer metabolism, and the road ahead, EMBO Rep. 17 (2016) 1721–1730, https://doi.org/10.15252/embr.201643300.
[55] P.S. Ward, C.B. Thompson, Metabolic reprogramming: a cancer hallmark even Warburg did not anticipate, Cancer Cell 21 (2012) 297–308, https://doi.org/10.1016/j.ccr.2012.02.014.
[56] K. Bluemlein, N.-M. Grüning, R.G. Feichtinger, H. Lehrach, B. Kofler, M. Ralser, No evidence for a shift in pyruvate kinase PKM1 to PKM2 expression during tumorigenesis, Oncotarget 2 (2011) 393–400, https://doi.org/10.18632/oncotarget.278.
[57] S. Desai, M. Ding, B. Wang, Z. Lu, Q. Zhao, K. Shaw, W.K.A. Yung, J.N. Weinstein, M. Tan, J. Yao, Tissue-specific isoform switch and DNA hypomethylation of the pyruvate kinase PKM gene in human cancers, Oncotarget 5 (2014) 8202–8210, https://doi.org/10.18632/oncotarget.1159.
[58] C. Zhan, L. Yan, L. Wang, J. Ma, W. Jiang, Y. Zhang, Y. Shi, Q. Wang, Isoform switch of pyruvate kinase M1 indeed occurs but not to pyruvate kinase M2 in human tumorigenesis, PLoS One 10 (2015) e0118663, https://doi.org/10.1371/journal.pone.0118663.
[59] H. Zhu, H. Luo, X. Zhu, X. Hu, L. Zheng, X. Zhu, Pyruvate kinase M2 (PKM2) expression correlates with prognosis in solid cancers: a meta-analysis, Oncotarget 8 (2017) 1628–1640, https://doi.org/10.18632/oncotarget.13703.
[60] C. Feng, Y. Gao, C. Wang, X. Yu, W. Zhang, H. Guan, Z. Shan, W. Teng, Aberrant overexpression of pyruvate kinase M2 is associated with aggressive tumor features and the BRAF mutation in papillary thyroid cancer, J. Clin. Endocrinol. Metab. 98 (2013) E1524–E1533, https://doi.org/10.1210/jc.2012-4258.
[61] G. Yu, W. Sun, Y. Shen, Y. Hu, H. Liu, W. Li, Y. Wang, PKM2 functions as a potential oncogene and is a crucial target of miR-148a and miR-326 in thyroid tumorigenesis, Am. J. Transl. Res. 10 (2018) 1793–1801, http://www.ncbi.nlm.nih.gov/pubmed/30018720.
[62] G.M. Howell, S.P. Hodak, L. Yip, RAS mutations in thyroid cancer, The Oncologist 18 (2013) 926–932, https://doi.org/10.1634/theoncologist.2013-0072.
[63] Z. Duan, D.E. Lamendola, R.Z. Yusuf, R.T. Penson, F.I. Preffer, M.V Seiden, Overexpression of human phosphoglycerate kinase 1 (PGK1) induces a multidrug resistance phenotype, Anticancer Res.. 22 (n.d.) 1933–1941.
[64] D. Zieker, I. Königsrainer, I. Tritschler, M. Löffler, S. Beckert, F. Traub, K. Nieselt, S. Bühler, M. Weller, J. Gaedcke, R.S. Taichman, H. Northoff, B.L.D.M. Brücher, A. Königsrainer, Phosphoglycerate kinase 1 a promoting enzyme for peritoneal dissemination in gastric cancer, Int. J. Cancer 126 (2010) 1513–1520, https://doi.org/10.1002/ijc.24835.
[65] T.-L. Hwang, Y. Liang, K.-Y. Chien, J.-S. Yu, Overexpression and elevated serum levels of phosphoglycerate kinase 1 in pancreatic ductal adenocarcinoma, Proteomics 6 (2006) 2259–2272, https://doi.org/10.1002/pmic.200500345.
[66] S. Guo, Y. Xiao, D. Li, Q. Jiang, L. Zhu, D. Lin, H. Jiang, W. Chen, L. Wang, C. Liu, W. Fang, L. Lin, PGK1 and GRP78 overexpression correlates with clinical significance and poor prognosis in Chinese endometrial cancer patients, Oncotarget 9 (2018) 680–690, https://doi.org/10.18632/oncotarget.23090.
[67] H. Xie, G. Tong, Y. Zhang, S. Liang, K. Tang, Q. Yang, PGK1 drives hepatocellular carcinoma metastasis by enhancing metabolic process, Int. J. Mol. Sci. 18 (2017) 1630, https://doi.org/10.3390/ijms18081630.
[68] J. Wang, J. Wang, J. Dai, Y. Jung, C.-L. Wei, Y. Wang, A.M. Havens, P.J. Hogg, E.T. Keller, K.J. Pienta, J.E. Nor, C.-Y. Wang, R.S. Taichman, A glycolytic mechanism regulating an angiogenic switch in prostate cancer, Cancer Res. 67 (2007) 149–159, https://doi.org/10.1158/0008-5472.CAN-06-2971.
[69] D. Zieker, I. Königsrainer, J. Weinreich, S. Beckert, J. Glatzle, K. Nieselt, S. Bühler, M. Löffler, J. Gaedcke, H. Northoff, J.G. Mannheim, S. Wiehr, B.J. Pichler, C. von Weyhern, B.L.D.M. Brücher, A. Königsrainer, Phosphoglycerate kinase 1 promoting tumor progression and metastasis in gastric cancer - detected in a tumor mouse model using positron emission tomography/magnetic resonance imaging, Cell. Physiol. Biochem. 26 (2010) 147–154, https://doi.org/10.1159/000320545.
[70] X. Li, Y. Jiang, J. Meisenhelder, W. Yang, D.H. Hawke, Y. Zheng, Y. Xia, K. Aldape, J. He, T. Hunter, L. Wang, Z. Lu, Mitochondria-translocated PGK1 functions as a protein kinase to coordinate glycolysis and the TCA cycle in tumorigenesis, Mol. Cell 61 (2016) 705–719, https://doi.org/10.1016/j.molcel.2016.02.009.
[71] X. Qian, X. Li, Q. Cai, C. Zhang, Q. Yu, Y. Jiang, J.-H. Lee, D. Hawke, Y. Wang, Y. Xia, Y. Zheng, B.-H. Jiang, D.X. Liu, T. Jiang, Z. Lu, Phosphoglycerate kinase 1 phosphorylates Beclin1 to induce autophagy, Mol. Cell 65 (2017), https://doi.org/10.1016/j.molcel.2017.01.027 917–931.e6.
[72] P. Peruzzo, M. Comelli, E. Di Giorgio, E. Franforte, I. Mavelli, C. Brancolini, Transformation by different oncogenes relies on specific metabolic adaptations, Cell Cycle 15 (2016) 2656–2668, https://doi.org/10.1080/15384101.2016.1215387.
[73] R. Ralhan, J. Veyhl, S. Chaker, J. Assi, A. Alyass, A. Jeganathan, R.T. Somasundaram, C. MacMillan, J. Freeman, A.D. Vescan, I.J. Witterick, P.G. Walfish, Immunohistochemical subcellular localization of protein biomarkers distinguishes benign from malignant thyroid nodules: potential for fine-needle aspiration biopsy clinical application, Thyroid 25 (2015) 1224–1234, https://doi.org/10.1089/thy.2015.0114.
[74] Y. Ucal, M. Eravci, F. Tokat, M. Duren, U. Ince, A. Ozpinar, Proteomic analysis reveals differential protein expression in variants of papillary thyroid carcinoma, EuPA Open Proteomics 17 (2017) 1–6, https://doi.org/10.1016/j.euprot.2017.09.001.
[75] T.H. Patwa, C. Li, L.M. Poisson, H.-Y. Kim, M. Pal, D. Ghosh, D.M. Simeone, D.M. Lubman, The identification of phosphoglycerate kinase-1 and histone H4 autoantibodies in pancreatic cancer patient serum using a natural protein microarray, Electrophoresis 30 (2009) 2215–2226, https://doi.org/10.1002/elps.200800857.
[76] The Cancer Genome Atlas Research Network, Integrated genomic characterization of pancreatic ductal adenocarcinoma, Cancer Cell 32 (2017), https://doi.org/10.1016/j.ccell.2017.07.007 185–203.e13.
[77] S. Shukla, R.B. Govekar, R. Sirdeshmukh, C.S. Sundaram, A.K. D'Cruz, K.A. Pathak, S.V. Kane, S.M. Zingde, Tumor antigens eliciting autoantibody response in cancer of

gingivo-buccal complex, Proteomics Clin. Appl. 1 (2007) 1592–1604, https://doi.org/10.1002/prca.200700206.
[78] J.J. Ladd, T. Chao, M.M. Johnson, J. Qiu, A. Chin, R. Israel, S.J. Pitteri, J. Mao, M. Wu, L.M. Amon, M. McIntosh, C. Li, R. Prentice, N. Disis, S. Hanash, Autoantibody signatures involving glycolysis and splicesome proteins precede a diagnosis of breast cancer among postmenopausal women, Cancer Res. 73 (2013) 1502–1513, https://doi.org/10.1158/0008-5472.CAN-12-2560.
[79] E.C. Farlow, K. Patel, S. Basu, B.-S. Lee, A.W. Kim, J.S. Coon, L.P. Faber, P. Bonomi, M.J. Liptay, J.A. Borgia, Development of a multiplexed tumor-associated autoantibody-based blood test for the detection of non-small cell lung cancer, Clin. Cancer Res. 16 (2010) 3452–3462, https://doi.org/10.1158/1078-0432.CCR-09-3192.
[80] K.S. Looi, E.S. Nakayasu, R.A. de Diaz, E.M. Tan, I.C. Almeida, J.-Y. Zhang, Using proteomic approach to identify tumor-associated antigens as markers in hepatocellular carcinoma, J. Proteome Res. 7 (2008) 4004–4012, https://doi.org/10.1021/pr800273h.
[81] M. Forgber, U. Trefzer, W. Sterry, P. Walden, Proteome serological determination of tumor-associated antigens in melanoma, PLoS One 4 (2009) e5199, https://doi.org/10.1371/journal.pone.0005199.
[82] T. Stasyk, L.A. Huber, Zooming in: fractionation strategies in proteomics, Proteomics 4 (2004) 3704–3716, https://doi.org/10.1002/pmic.200401048.